Journal of Solid State Chemistry 184 (2011) 2909–2919

Contents lists available at SciVerse ScienceDirect

Journal of Solid State Chemistry

journal homepage: www.elsevier.com/locate/jssc

A general solution-chemistry route to the synthesis Li*M*PO_4 (*M*=Mn, Fe, and Co) nanocrystals with [010] orientation for lithium ion batteries

Jing Su [a], Bing-Qing Wei [b], Jie-Peng Rong [b], Wen-Yan Yin [a], Zhi-Xia Ye [a], Xian-Qing Tian [a], Ling Ren [a,*], Min-Hua Cao [a,*], Chang-Wen Hu [a]

[a] Key Laboratory of Cluster Science, Ministry of Education of China, Department of Chemistry, Beijing Institute of Technology, Beijing 100081, PR China
[b] Department of Mechanical Engineering, University of Delaware, Newark, DE 19716, USA

ARTICLE INFO

Article history:
Received 28 April 2011
Received in revised form
2 July 2011
Accepted 14 August 2011
Available online 8 September 2011

Keywords:
Ethanol solvothermal route
Li*M*PO_4 microstructures
Lithium-ion batteries

ABSTRACT

A general and efficient solvothermal strategy has been developed for the preparation of lithium transition metal phosphate microstructures ($LiMnPO_4$, $LiFePO_4$, and $LiCoPO_4$), employing ethanol as the solvent, LiI as the Li source, metal salts as the M sources, H_3PO_4 as the phosphorus source, and poly(vinyl pyrrolidone) (PVP) as the carbon source and template. This route features low cost, environmental benign, and one-step process for the cathode material production of Li-ion batteries without any complicated experimental setups and sophisticated operations. The as-synthesized Li*M*PO_4 microstructures exhibit unique, well-shaped and favorable structures, which are self-assembled from microplates or microrods. The *b* axis is the preferred crystal growth orientation of the products, resulting in a shorter lithium ion diffusion path. The $LiFePO_4$ microstructures show an excellent cycling stability without capacity fading up to 50 cycles when they are used as a cathode material in lithium-ion batteries.

1. Introduction

Lithium ion batteries (LIBs) have been spectacular in the past decade because of their appealing advantages, such as a high operative voltage and high energy density, long cycling life, no memory effect, negligible self-discharge, and so on, compared with other rechargeable cells. Therefore, they are critical power sources for portable electronic devices like cell phones, camcorders or lap-top computers, and even for electric vehicle applications. However, the commercial LIBs currently are based on layered $LiCoO_2$ cathode material, which generally suffer from relatively low capacity [1] and safety concerns upon overcharge [2]. In an intensive exploration for alternative cathode materials, olivine type phosphates have emerged since the pioneering work of Padhi and his co-workers [3], i.e. $LiMnPO_4$ and $LiFePO_4$, as well as the mixed phases ($LiFe_xMn_{1-x}PO_4$ ($0<x<1$)), due to their inherent features such as environmental friendliness, economic viability, thermal stability, and abundant availability.

From a structural viewpoint, one intuitively expects that lithium ion diffusion should be one-dimensional. Olivine-Li*M*PO_4 (*M*=Mn, Fe, and Co) has orthorhombic crystalline phase with a space group of *Pnma*. It adopts a slightly distorted hexagonal close-packed oxygen array and the crystal skeleton consists of MO_6 octahedra and PO_4 tetrahedra, in which M and Li occupy different octahedral interstitial sites. More specifically, the divalent transition metal atom nestles in the *M*2(010) site to form plane of corner-shared octahedra in the *bc* plane, phosphorus locates in tetrahedral site, and lithium resides in the *M*1(100) site to generate linear chain of edge-sharing octahedra along the direction of the *b*-axis, where the one-dimensional diffusion of Li^+ ion takes place during charge and discharge [4], and the charge transfer occurs mainly on the *ac*-plane, that is (020) plane [5]. These chains are bridged by edge and corner shared phosphate tetrahedra, to build a rigid three-dimensional structure as shown in Fig. 1A. On the one hand, because of the inductive effect of the M–O–P linkage [6,7], the energy of M^{3+}/M^{2+} couple is adjusted to a value, which is much lower than that in oxides, related to the Fermi energy of lithium metal, generating much greater redox potential with respect to Li^+/Li. The $LiFePO_4$ operates at a flat voltage of 3.4 V versus Li^+/Li, yielding a moderately theoretical discharge capacity of 170 mA h g^{-1}. In addition, the other phosphates with Mn^{3+}/Mn^{2+} and Co^{3+}/Co^{2+} couples are tuned to 4.1 and 4.8 V [8,9], respectively, providing the possibility to increase the energy and power density. On the other hand, the large PO_4^{3-} polyanion separates the chain of FeO_6 edge-shared octahedra, leading to extremely poor electronic conductivity and small lithium ion diffusion coefficient, which may result in a loss of capacity during high-rate discharge. Therefore, how to improve

* Corresponding authors. Fax: +86 10 68912631.
E-mail address: caomh@bit.edu.cn (M.-H. Cao).

0022-4596/$ - see front matter © 2011 Elsevier Inc. All rights reserved.
doi:10.1016/j.jssc.2011.08.042

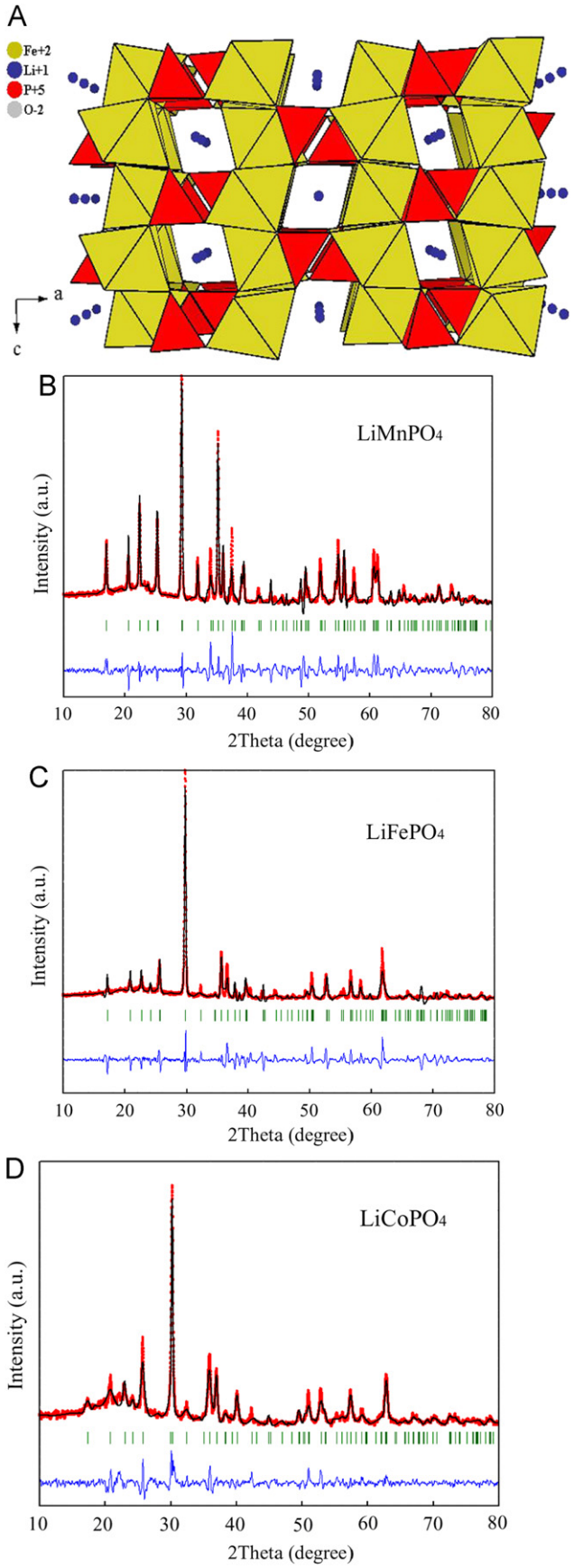

Fig. 1. (A) The olivine-$LiFePO_4$ structure in space group *Pnma*, (B) XRD patterns of the $LiMPO_4$ (M=Mn, Fe, and Co) microstructures obtained by the solvothermal process along with the Rietveld fits; ●: observed XRD pattern; —: calculated XRD pattern; ——: difference between observed and calculated patterns; |: Bragg position.

transfer rate of electron in olivine structure is vital for the commercial applications of $LiMPO_4$. Tremendous attempts have been devoted in recent years to circumvent these impediments by cationic doping [10–12], minimizing the particle size through suitable preparation routes [13–17], or coating with conducting materials (typically carbon, metals, metal oxides, phosphide, polymers, etc.) [18–24]. Besides, the crystal orientation of the $LiMPO_4$ particles has also a significant effect on the electrochemical reaction processes as a result of their anisotropic crystal structure [25]. Recent research demonstrates that the Li^+ ion diffusion across the surface is as significant as electron transport: Li^+ can easily move only in the tunnels parallel to the *b* direction as aforementioned, although $LiMPO_4$ can exchange Li^+ with the electrolyte on all surface facets of the bulk in principle [26,27]. Hence, increasing diffusion along the surface towards the (010) facet is another alternative to enhance rate capability.

To the best of our knowledge, among the various synthetic approaches proposed in the past decade, the most conventional and traditional synthesis of metal olivine phosphates involves high-temperature solid-state reaction in inert atmospheres (for example, $Ar–H_2$ mixture). To obtain relative satisfactory product, this method entails several complicated synthesis steps (including grinding, ball milling, and subsequent calcining treatment generally at 400–700 °C) for a long time until the crystals formed at the expense of energy and inert gas [28–30]. However, these severe conditions preclude subtle control on size and shape of the final products. Therefore, solution-techniques, such as direct precipitation route [6], sol–gel method [31], and solution process based synthesis [32–39] emerged recently as a result of the need of small particle size $LiMPO_4$. The solution methods have been proven to be particularly successful for the control for final products and they are more versatile with regard to particle morphology, due to the broadness of these approaches. However, for the sol–gel procedure, even though it is capable of obtaining gel precursors, in which multiple starting ingredients are intimately mixed at the atomic level, thus resulting in finer particles of high purity, it still requires an additional post heat-treatment process to obtain crystalline $LiMPO_4$. Furthermore, the aqueous-based synthesis can cause the oxidation of Fe^{2+} to Fe^{3+}, which may lead to the formation of impurity phase like Fe_2O_3, although it can be controlled by some cumbersome ways, for instance, adding reducing agents, adjusting the pH value of reacting system or carrying out under inert gas flow. Apart from $LiMPO_4$ powders, there are several reports on the preparation of the olivine $LiMPO_4$ thin-films by physical deposition methods [40,41]. However, these olivine thin-film cathodes exhibited a low capacity. Therefore, it is critical to develop a simple, economic, and efficient route for the synthesis of $LiMPO_4$ materials.

In recent years, ethanol-based solvothermal technique has been proven to be a successful means to prepare various micro- and nano-structured materials, and it has notable virtues such as simple and straightforward operations, cost-effectiveness, and scalable production. Up to now, micro- and nano-structures of relatively simple compounds, such as Mn_2O_3 [42], CoO [43], WO_3 [44], and ZnS [45] have been solvothermally synthesized using ethanol as the solvent. Cathode active materials, i.e., LiV_2O_5 nanorods [46] and Li–Ti–O [47] nanocrystals, have also been synthesized using this method. However, there have been no reports on the general synthesis of multi-component materials such as $LiMPO_4$ via the ethanol solvothermal systems.

With this perspective, a solvothermal process is used to establish a general, novel, and facile strategy for the preparation of $LiMPO_4$ (M=Mn, Fe, and Co) microstructures at a low temperature, using ethanol as the "green" solvent, LiI as the lithium source, transitional metal salt as the M sources, H_3PO_4 as the phosphorous source, and poly(vinyl pyrrolidone) (PVP) as the carbon source and template. Compared with the above-mentioned

methods, the present route has some intriguing advantages: (1) ethanol solvent route is able to overcome many of mentioned-above specific problems typical for aqueous systems and solid state reaction systems. For example, because of the low solubility of oxygen in the solvothermal system, it provides an inert atmosphere for the synthesis of Li*M*PO_4, without additional of any gaseous protection during the reaction process; (2) all precursors used in our experiment could be readily dissolved in ethanol, in which a molecular level mixing for the reaction system has been achieved, offering high purity and homogeneity, and low processing temperatures; and (3) it is a successful means to generate microstructured materials with unique and favorable particle morphologies, which are self-assembled by microplates or microrods. Moreover, the crystal orientation with (020) texture of the as-prepared Li*M*PO_4 microstructures are obtained, in which electrochemical reaction can be accelerated, and the electrochemical activity of the $LiFePO_4$ microstructures is investigated.

2. Experimental

2.1. Materials

All chemicals used were purchased without further purification. $Mn(CH_3COO)_2 \cdot 4H_2O$ was from Beijing Chemical Reagents Company; $FeCl_3 \cdot 6H_2O$ was from Beijing Yili Fine Chemical Co., Ltd; $Co(CH_3COO)_2 \cdot 4H_2O$ was from Sinopharm Chemical Reagent Co., Ltd; LiI was from Shanghai China Lithium Industrial Co., Ltd; poly(vinyl pyrrolidone) (PVP) (K30) was from Beijing Chemical plant; ethanol was from Tianjin Fuchen Chemical Reagents Company; H_3PO_4 (85 wt% solution) was from Beijing Chemical plant.

2.2. Synthesis

The Li*M*PO_4 microstructures were prepared by a simple and mild solvothermal approach in the presence of PVP as described below. The respective salts of Mn, Fe, or Co [$Mn(CH_3COO)_2 \cdot 4H_2O$, $FeCl_3 \cdot 6H_2O$, $Co(CH_3COO)_2 \cdot 4H_2O$], LiI, and PVP were dissolved in ethanol. H_3PO_4 (85 wt% solution) was then added to the reaction mixture at room temperature to realize a molar ratio of Li:M:P:PVP=10:1:1.5:7. After vigorous magnetic stirring at room temperature for 0.5 h, the homogeneous light-yellow transparent solution formed for *M*=Mn, wine-colored solution for *M*=Fe, and violet solution for *M*=Co were transferred into three 100 mL Teflon-lined stainless steel autoclaves, respectively, which were heated at 180 °C for 2 days. After cooled to room temperature naturally, the resulting milk-white $LiMnPO_4$, green-gray $LiFePO_4$, and purple $LiCoPO_4$ precipitation were centrifugated and washed repeatedly using distilled water and absolute alcohol. The obtained powder was then dried in air for 8 h.

2.3. Characterization

X-ray powder diffraction (XRD) characterization of the resulting products were carried out with a SHIMADZU XRD-6000 X-ray power diffraction with Cu-*K*α radiation (λ=1.54056 Å) at 40 kV and 50 mA. The morphology and microstructure of the samples were observed using field emission scanning electron microscopy (FE-SEM, JEOL S-4800) and the transmission electron microscopy (TEM, H-8100). Details of the samples microstructures were determined using high-resolution transmission electron microscopy (HRTEM) on a JEM-2010 apparatus with an acceleration voltage of 200 kV. The Fourier transform infrared spectroscopy (FT-IR) patterns were recorded with a Nicolet 170SXFT/IR spectrometer using KBr pressed wafers to test the chemical bonding of the products from 400 to 2000 cm^{-1}. The oxidation states of metal ions were confirmed by the X-ray photoelectron spectroscopy (XPS) measurements, carrying out on an ESCALAB 250 instrument and using Al *K*α irradiation. Elemental compositions of the compound powder were determined by EDAX and the amount of carbon was examined by the element analyzer (Vario EI, Germany).

2.4. Electrochemical measurements

The electrochemical performance of the microsized $LiFePO_4$ as the cathode was evaluated using CR2032 coin cells assembled in an argon-filled glove box. For the cathode preparation, a mixture of $LiFePO_4$ microcrystals, carbon black, and poly(vinyl difluoride) (PVDF) with a weight ratio of 70/20/10 was pasted on an Al foil, which works as a current collector. A Celgard 2340 microporous membrane was used as the separator and lithium foil was used as the counter electrode. The non-aqueous electrolyte was 1 M $LiPF_6$ in a 1:1 (in wt%) mixture of ethylene carbonate (EC)/dimethyl carbonate (DMC) obtained from Ferro Corporation. A galvanostatic cycling test of the cells was performed between 2.5 and 4.2 V vs. Li^+/Li with an Arbin BT4 (Arbin Instruments, BT4, USA), where the C-rate is based on the theoretical capacity of $LiFePO_4$ (170 mA h g^{-1}). All cells were tested at room temperature.

3. Results and discussion

Chemical synthesis by solvothermal approach is very efficient and energy saving, since it offers rapid heating, high reaction rate and selectivity. The general route can be used to prepare a series of lithium metal phosphate (*M*=Mn, Fe, and Co) microstructures. In this low temperature-controlled solvothermal process, without the use of any organic reducing agent and inert gas protection, the homogeneous reaction atmosphere could create a uniform nucleation condition, thus, the production of Li*M*PO_4 crystals with a narrow size distribution is feasible.

3.1. Structural characterization

Fig. 1B–D display the experimental XRD patterns of the $LiMnPO_4$, $LiFePO_4$, and $LiCoPO_4$ samples together with the respective Rietveld refinement. All of the reflections could be assigned to an orthorhombic olivine-type structure with the *Pnma* space group (Fig. 1A), indicating the formation of pure $LiMnPO_4$ (JCPDS card no. 77-0178), $LiFePO_4$ (JCPDS 81-1173), and $LiCoPO_4$ (JCPDS 85-0002) samples. The sharp diffraction peaks without those for any impurity phases such as Li_3PO_4 and others, which often appear in the Li*M*PO_4 product synthesized by traditional routes [48], illustrate the highly crystalline nature of Li*M*PO_4 achieved by the solvothermal process at a low temperature of 180 °C. Moreover, it can be clearly seen that the XRD peak positions in Fig. 1B–D gradually shift to higher angles from *M*=Mn to Fe to Co because the ionic radius for these three elements follows the order $Mn^{2+} > Fe^{2+} > Co^{2+}$. The experimental powder diagram and the pattern calculated by Rietveld refinement agree well with each other, confirming the structural model.

Ceder et al. [49] ever reported that the Li^+ migration energy of the (010) channel in vacuum is less than those of other axes. It is considered that the surface energy of the *ac*-plane is lower than that of other crystal planes under solvothermal conditions and the crystal growth of the product would proceed to diminish the surface energy and match up the minimum energy criterion. This is significant as this orientation is the easiest pathway for lithium motion in the material, as anticipated by consideration of the texture, and as calculated through computational models and first

principle methods by Morgan et al. [25]. More recently, Nishimura group [50] have firstly pointed out that a curved one-dimensional chain for lithium mobility along the [010] direction has been clearly confirmed by combining the maximum entropy and high-temperature powder neutron diffraction method. Therefore, there is of great interest in synthesizing phospho-olivines dominantly with the [020] direction to be the shortest dimension in the crystals. However, in our case, it should be noted that the (020) peaks for these three sample at 29.8° in Fig. 1B are much more intense, which provides such a possibility that our as-synthesized samples may possess such a perfect structure above mentioned. Exact crystal growth orientation for our samples will be determined by high resolution transmission electron microscopy (HRTEM) result below.

To further investigate the oxidation states of Fe, Mn, and Co in the LiMPO$_4$ (M=Mn, Fe, and Co) samples, surface analysis was carried out using XPS. Fig. 2 shows the wide XPS spectra and the M 2p XPS spectra (M=Mn, Fe, and Co) of these three samples. From Fig. 2a, c, and e it can be seen that the binding energy of Li 1s, P 2p, and O 1s for these samples are almost same and they are determined to be nearly 55.4, 143.0, and 532.7 eV, respectively, with the binding energy at 284.4 eV for the C 1s peak. For LiMnPO$_4$ sample, the high resolution Mn 2p spectrum shows two peaks with binding energy of 641.8 and 653.9 eV in Fig. 2b, indicating that the oxidation state of Mn is +2 [51]. The binding energy positions at 711.8 and 725.1 eV for the Fe 2p spectrum as shown in Fig. 2d are ascribed to Fe2$p_{3/2}$ and Fe2$p_{1/2}$, respectively, which are characteristic of Fe^{2+}, perfectly in agreement with

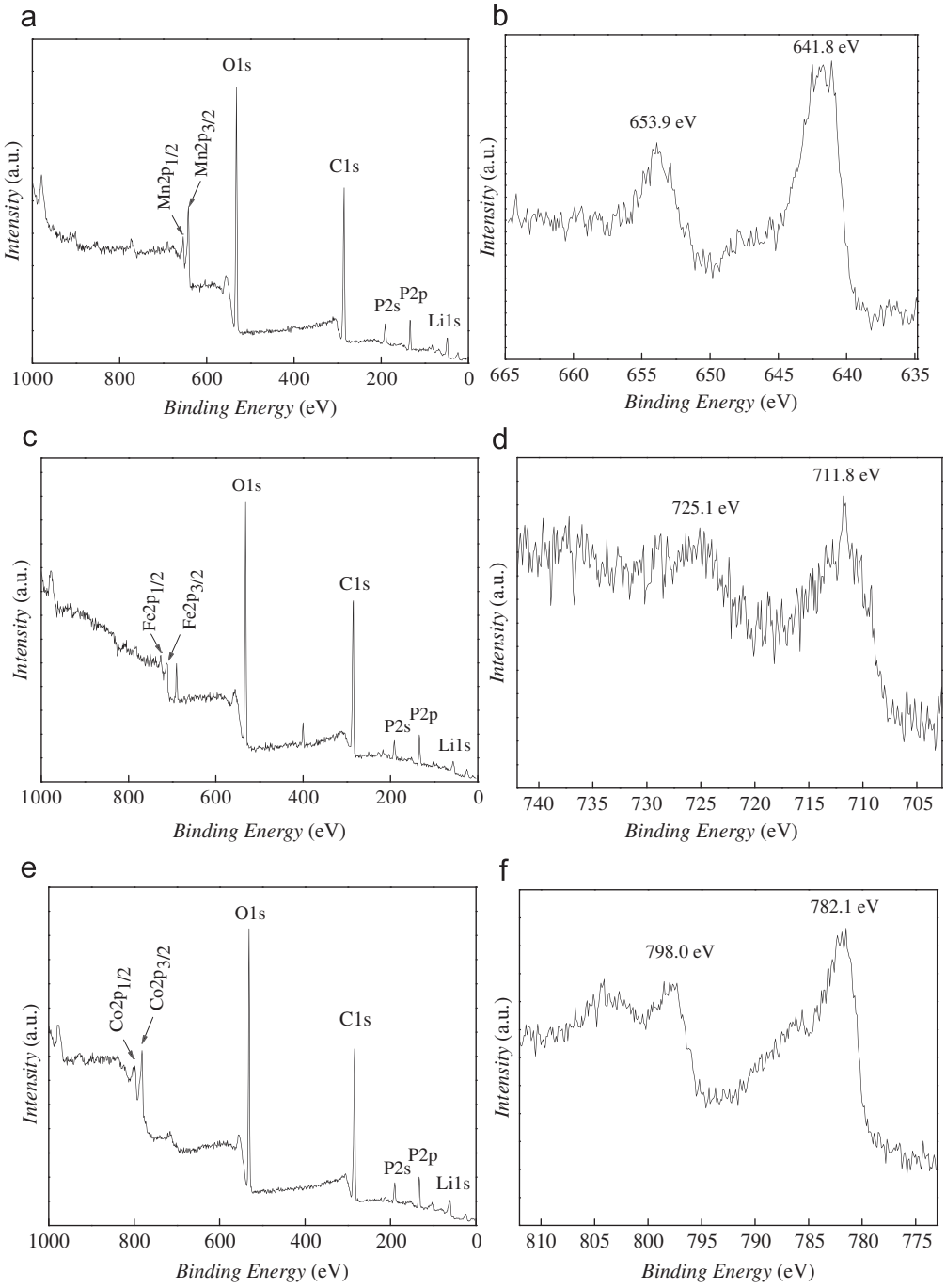

Fig. 2. Wide XPS spectrum and M 2p XPS spectrum of the LiMPO$_4$ (M=Mn, Fe, and Co) samples: (a, b) for LiMnPO$_4$; (c, d) for LiFePO$_4$; and (e, f) for LiCoPO$_4$.

previously reported spectra of $LiFePO_4$ [52a]. Fig. 2f shows two peaks of Co 2*p* with binding energies of 781.2 and 798.0 eV, in consistency with Co^{2+} [52b], indicating that the oxidation state of Co in $LiCoPO_4$ is also +2. Therefore, the XPS analyses confirm the high purity of Li*M*PO_4 samples.

3.2. Microstructural characterization

The size and shape of the as-prepared Li*M*PO_4 were firstly examined by typical low-magnification field emission scanning electron microscopy (FE-SEM). Fig. 3 shows the FE-SEM images of $LiMnPO_4$ samples with different additives. As shown in Fig. 3a, the FE-SEM image of the $LiMnPO_4$ sample obtained in the presence of polyvinyl pyrrolidone (PVP), indicates that the sample almost completely consists of rod-like nanostructures, which are not uniform with a diameter of ~50 nm and length about ~5 μm. Moreover, it can be clearly observed that most of these whiskers exhibit non-uniform diameters along the growth direction. This morphology of $LiMnPO_4$ sample is completely different from $LiMnPO_4$ two dimensional nanoplates synthesized via a solid-state reaction in molten hydrocarbon and a polyol method, respectively [39,53a].

To evaluate the impact of PVP on the morphology of $LiMnPO_4$, we carried out a series of compared experiments, in which we only varied additives used (no additive, glucose, and poly (ethylene glycol) (PEG) 20000) and other reaction conditions were kept constant. When no additive or PEG-20000 was used, irregular particles were observed as shown in Fig. 3b and c. If glucose was used, the sample consists of three dimensional nanostructures (Fig. 3d), which have a smaller size than previous three cases. Thus it can be concluded that PVP plays an important role in the morphology control of $LiMnPO_4$. However, the amount of PVP has a little effect on both morphology and size of $LiMnPO_4$. The described process can completely be used to synthesize $LiFePO_4$ nanostructures. Fig. 4a shows a typical FE-SEM image of the as-synthesized $LiFePO_4$ sample, which is mainly composed of fan-shaped bundles, and the microbundles are constructed by rod-like nanostructures, further confirmed by TEM image (Fig. 7e). In this experiment, we have also attempted various conditions as those for $LiMnPO_4$. As shown in Fig. 4b–d, almost no morphology change was observed and only some small fractures besides integrated fan-shaped bundles existed in samples for these three cases. If transition metal cation was replaced by Co, pure $LiCoPO_4$ microstructures were obtained as shown in Fig. 5. Fig. 5a presents the perfect straw-like aggregates consisting of $LiCoPO_4$ needles obtained in the presence of PVP. Fig. 5b (the inset of Fig. 5a) shows a single straw-like structure, from which we can see that the $LiCoPO_4$ needles have an average diameter of less than 100 nm. Such a size is far less than that reported for $LiCoPO_4$ micron-rods with an average diameter of about 500 nm [53b]. However, the $LiCoPO_4$ samples appear evidently aggregated without PVP (Fig. 5c), even for the presence of glucose and PEG 20000 (Fig. 5d and e). Compared with the previous two cases, PVP has played a more important role in the morphology control for the synthesis of $LiCoPO_4$ microstructures.

However, this strategy could not be applied to another member of the Li*M*PO_4 series, $LiNiPO_4$. For example, we have conducted the experiment, in which $Ni(NO_3)_2 \cdot 6H_2O$ or $NiCl_2 \cdot 6H_2O$ was used as nickel source, and other conditions were kept same as those for Mn, Fe, and Co. $Ni_{11}(HPO_3)_8(OH)_6$ instead of $LiNiPO_4$ was obtained, as confirmed by the XRD pattern in Fig. 6a. The SEM images of the sample are shown in Fig. 6b and c. It can be disclosed that the three-dimensional microstructures assembled by the cross-connection of the microrods dominate and a few irregular particles are occasionally observed in the sample. We have tried to change a series of reaction conditions, but we did not get $LiNiPO_4$ that we expected, but $Ni_{11}(HPO_3)_8(OH)_6$. In fact, $LiNiPO_4$ is not typically used as a cathode material because of its higher oxidation potential [31], although $LiNiPO_4$ also forms the olivine structure [3]. Recently, transition metal phosphate have attracted extensive interests because of their microporous structures and novel potential applications

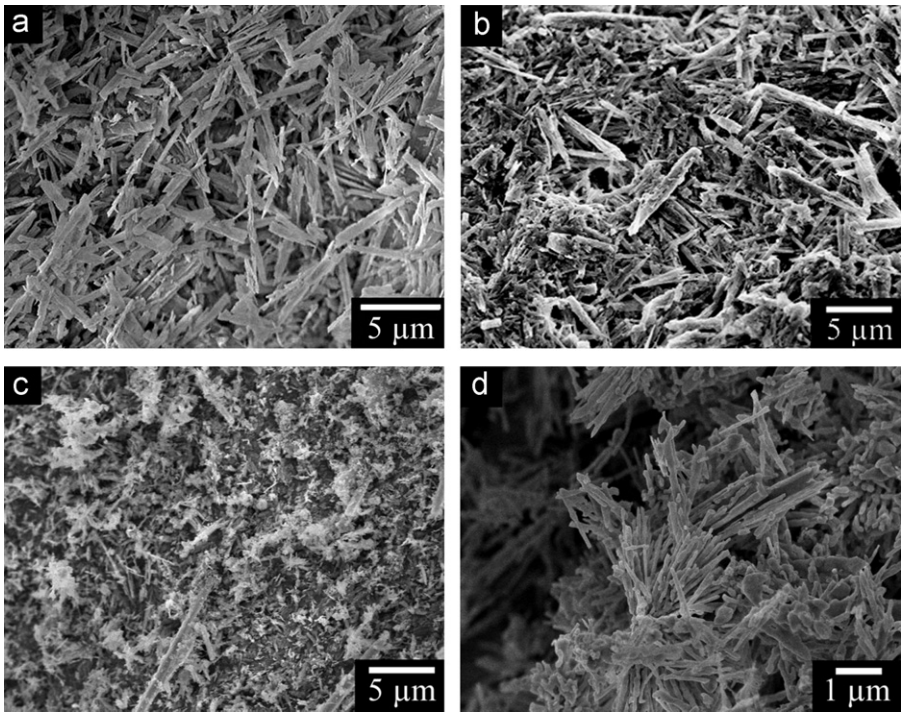

Fig. 3. SEM images of $LiMnPO_4$ microstructures obtained by the solvothermal process: (a) $LiMnPO_4$ with PVP, (b) $LiMnPO_4$ without any additive, (c) $LiMnPO_4$ with PEG 20000, and (d) $LiMnPO_4$ with glucose.

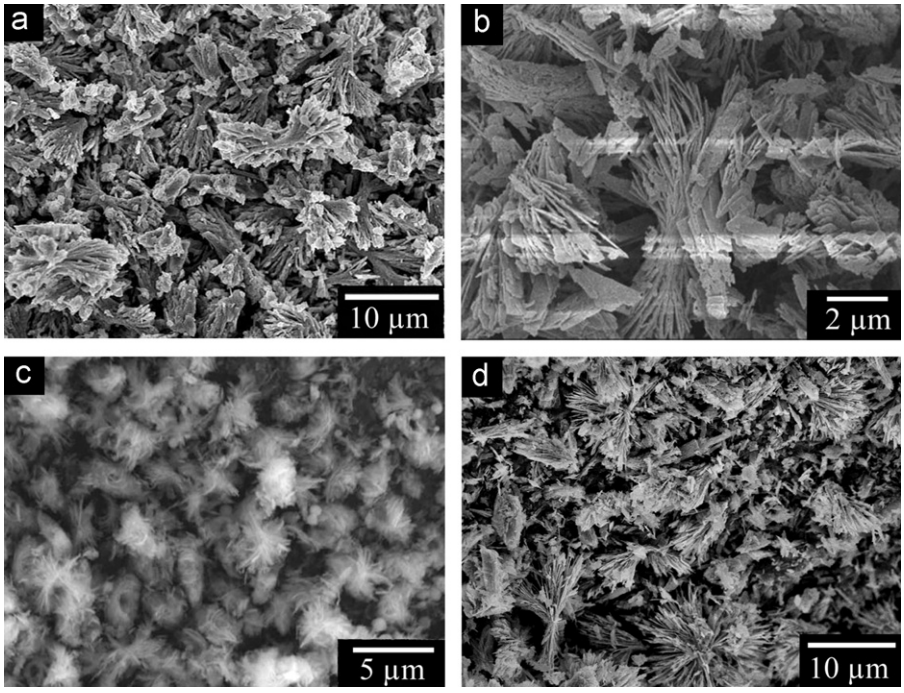

Fig. 4. SEM images of $LiFePO_4$ microstructures obtained by the solvothermal process: (a) $LiFePO_4$ with PVP, (b) $LiFePO_4$ without any additive, (c) $LiFePO_4$ with PEG 20000, and (d) $LiFePO_4$ with glucose.

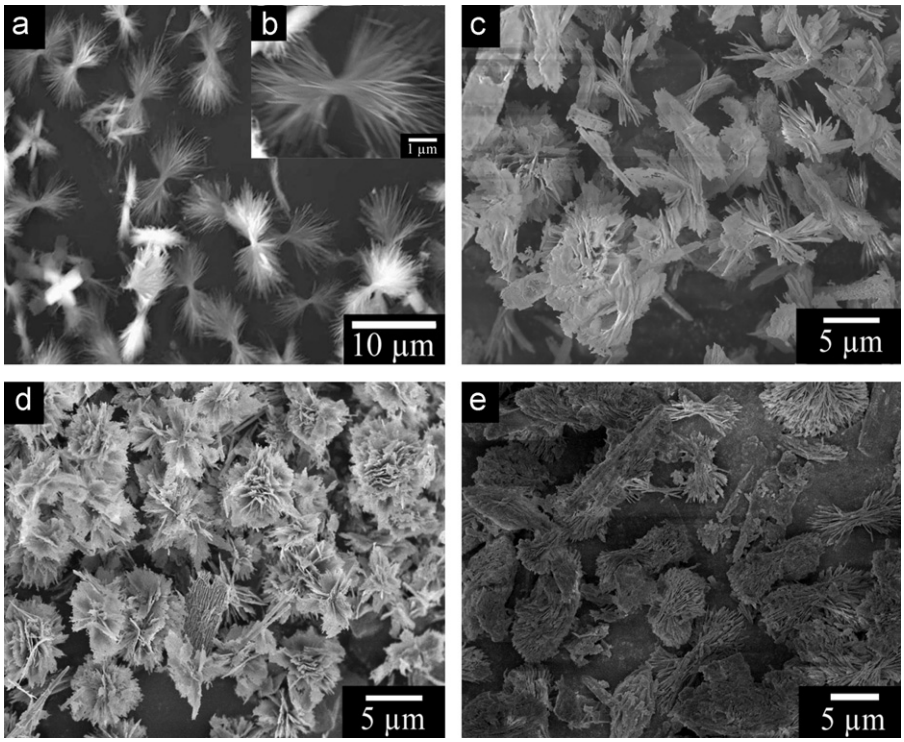

Fig. 5. SEM images of $LiCoPO_4$ microstructures obtained by the solvothermal process: (a, b) $LiCoPO_4$ with PVP, (c) $LiCoPO_4$ without any additive, (d) $LiCoPO_4$ with PEG 20000, and (e) $LiCoPO_4$ with glucose.

as catalysts, ion-exchangers, or molecular sieves. Therefore the as-synthesized $Ni_{11}(HPO_3)_8(OH)_6$ with controlled morphology and size may find their wide applications in the field of chemistry.

To better understand the microstructure and morphology of the as-synthesized Li*M*PO_4 products, transmission electron microscopy (TEM) observations of all samples were performed (Fig. 7). For all three cases, as clearly shown in Fig. 7a, e, and i, the building block consisting of the three-dimensional microstructures exhibits more evident rod-like nanostructures. It is worth mentioning that these microstructures are intact even under ultrasonic treatment, exhibiting excellent structural stability [54]. In addition, high-resolution TEM images taken on respective nanorods of the Li*M*PO_4 microstructures are shown in Fig. 7b, f, and j. All present clear crystal lattices with same *d*-spacing of 0.30 nm, corresponding to (020) planes of orthorhombic phase Li*M*PO_4, which are in well agreement with the XRD results discussed above. Such structures were expected

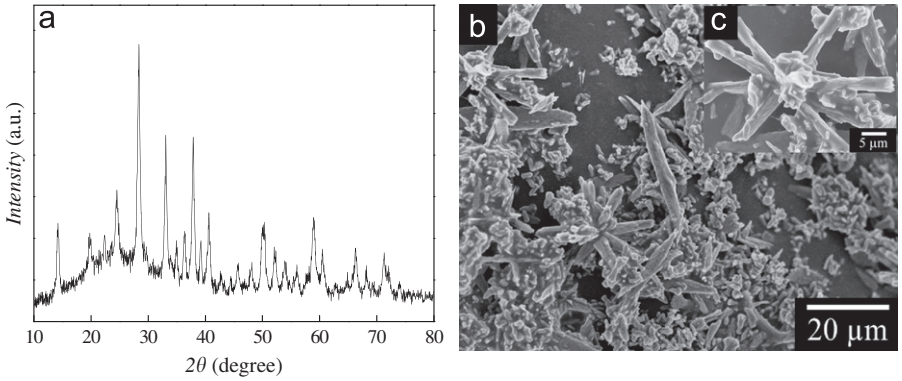

Fig. 6. (a) XRD pattern and (b, c) SEM image of $Ni_{11}(HPO_3)_8(OH)_6$ microstructures obtained by the solvothermal process.

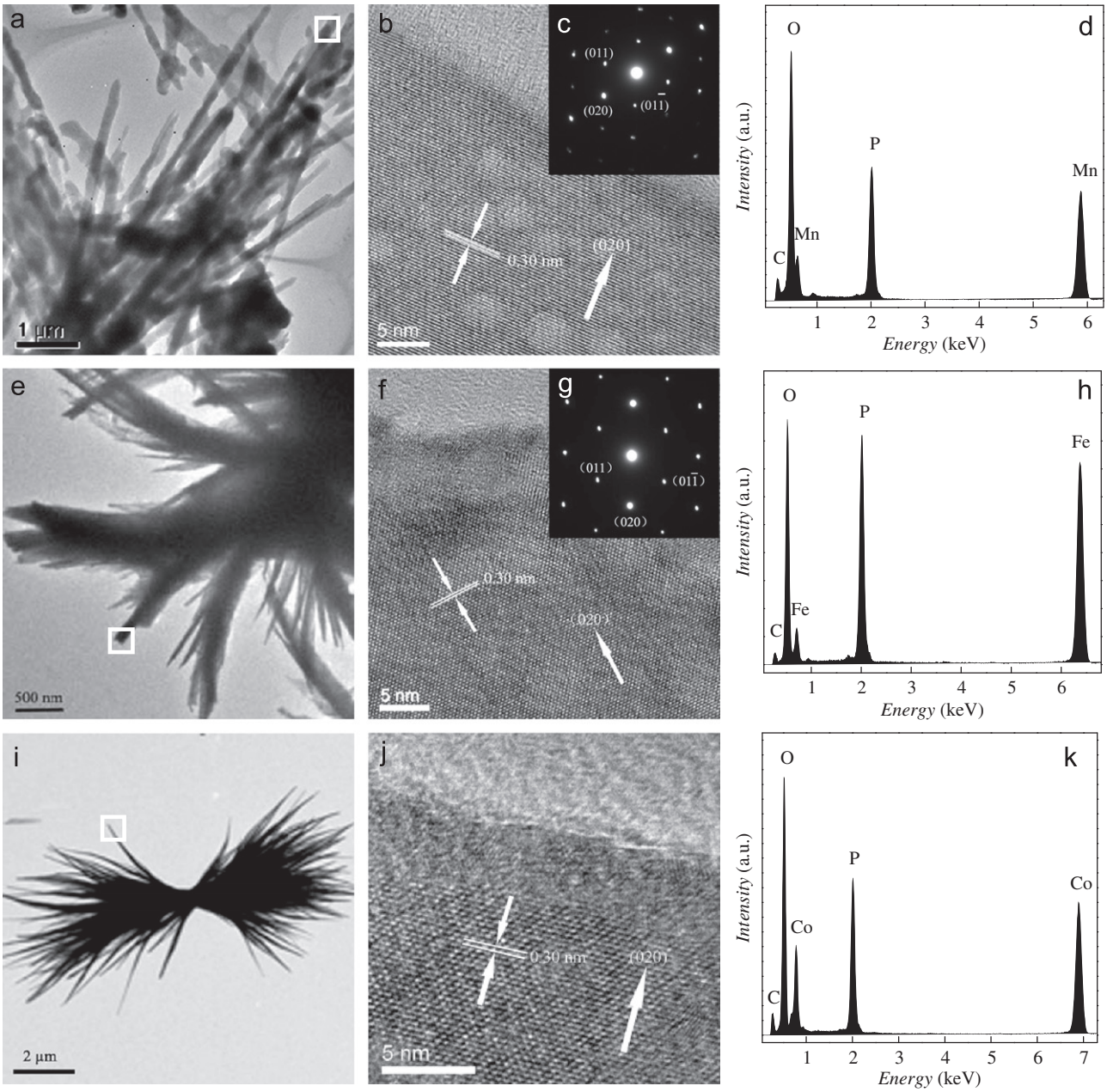

Fig. 7. Typical TEM images of LiMPO_4 (M=Mn, Fe, and Co) microstructures obtained by the solvothermal process: (a, b) $LiMnPO_4$; (e, f) $LiFePO_4$; (h, i) $LiCoPO_4$; (c, g) SAED patterns of $LiMnPO_4$ and $LiFePO_4$, respectively; (d, h, k) EDX patterns (red panes in a, e, h) of $LiMnPO_4$, $LiFePO_4$ and $LiCoPO_4$ samples.

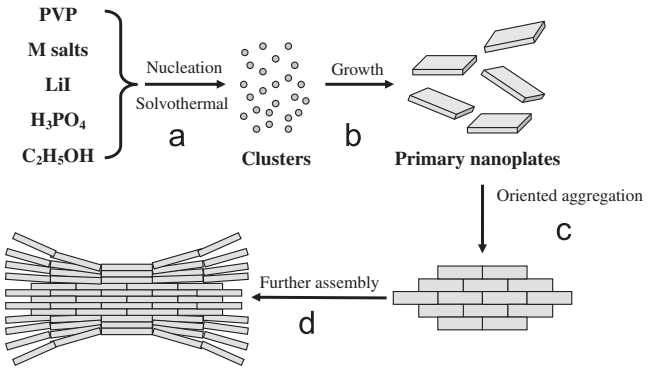

Fig. 8. Proposed formation mechanism of hierarchical nanostructures.

to have the easiest pathway for lithium motion, which is beneficial for the practical Li-ion battery applications. In addition, amorphous layers with several nanometers around Li*M*PO_4 crystal lattice can also be seen from the HRTEM images, which can be further confirmed by following infrared spectrum discussion. Except the $LiCoPO_4$ sample, which is unstable under electron beam, the selected area electron diffraction (SAED) patterns of other two samples are shown in Fig. 7c and g. For both samples, regular and clear diffraction spot array is obtained, indicating that $LiMnPO_4$ and $LiFePO_4$ microstructures are single-crystalline and exhibit preferential growth along the [020] direction, which is the long axis of the nanorods. Energy dispersive X-ray (EDX) patterns, as shown in Fig. 7d, h and k for $LiMnPO_4$, $LiFePO_4$, and $LiCoPO_4$, respectively, prove the presence of M, P, O, and C in the Li*M*PO_4 (*M*=Mn, Fe, and Co) products.

Compared with the texture and microstructure described in other literatures, we find that Li*M*PO_4 synthesized through solid-state reaction [29,30] and sol–gel method [14,31] are likely to grow into spherical or irregular fine particles. Nevertheless, generally, the Li*M*PO_4 samples prepared via hydrothermal [32–34] or solvothermal [38,55] route are crystallized in plate-like form, even further assembled into hierarchical microstructures, and have preferred crystal orientation with (020) texture. Consequently, in the present solvothermal process, possible formation mechanism of Li*M*PO_4 was proposed as schematically illustrated in Fig. 8. At the initial stage, numerous tiny crystalline nuclei appear in a supersaturated solution and then the crystal growth follows. With the reaction proceeding, these nuclei grow larger at the expense of the smaller ones, based on a well-known "Ostwald ripening process" (Fig. 8, step a) [56]. In the subsequent process, the particles diffused and aggregated together to form primary nanoplates (Fig. 8, step b). Afterwards, the nanoplates attached together and assembled in edge-to-edge and layer-by-layer growth style (Fig. 8, step c) [57]. Finally, instead of further piling up to form a column, the previously aggregated structures consisting of nanoplates preferred to tilt at both ends and form well-defined notched template, resulting in thickening of the edges and a stagnating growth in the middle section of structures (Fig. 8, step d). This specific growth way should be ascribed to surface interaction or lattice tension in the edge areas [58]. Thus, the self-assembled Li*M*PO_4 microstructures were formed, which is similar to the previous reports for the stacking process of Bi_2WO_6 [51] and some biomaterials [59].

The results discussed above suggest that the solvothermal method adopted for the synthesis of Li*M*PO_4 (*M*=Mn, Fe, and Co) can lead to hierarchical crystalline structures, which are mainly composed of rod-like nanostructures with length ranging from 5 to 10 μm, without subsequent heat treatments. It can also be concluded that PVP plays an important role in the morphology control of the final products. The large exposure of the electrochemically active crystal face of the thin profiles may reduce the length of lithium diffusion path and quicken the rate of electrochemical reaction process. In this way, the charge and discharge characteristics of Li*M*PO_4 should be discussed considering at least two factors, i.e., crystal texture and particle size.

3.3. Electrochemical properties

For potential application in Li-ion batteries, the electrochemical performances of the $LiFePO_4$ microstructures were examined in detail. Before the measurements of electrochemical properties, the as-synthesized microcomposite was annealed at 700 °C for 5 h (heating rate of 2 °C/min) under a mixed atmosphere of N_2 (90%) and H_2 (10%). The heat treatment, on the one hand, further crystallizes the sample obtained directly from the solvothermal method and on the other hand, transforms the remaining additive (PVP) into carbon to improve the electronic conductivity. XRD and SEM results (not shown) of the post-heated sample are similar to those of the before-heated one, illustrating that the heat treatment has no effect on the purity, morphology, and size of the sample. In addition, no reflections corresponding to the carbon are found in XRD pattern possibly due to its low content or its poor crystallinity. So, elemental analysis was performed to determine the carbon content of the post-heated sample. The mass percentage of carbon was determined by combustion elemental analysis to be 2 wt%. Therefore, hereafter the post-heated sample is referred to as $LiFePO_4$/C microcomposite. In addition, the presence of PVP in the before-heated sample and the interaction between PVP and Li*M*PO_4 crystal surfaces could be further confirmed by the Fourier transform infrared (FT-IR) spectroscopy. Fig. 9a shows the FT-IR spectrum of pure $LiFePO_4$ microstructures. The bands between 1080 and 945 cm^{-1} are attributed to the characteristic absorption of the PO_4^{3-}, and the bands at 637 and 545 cm^{-1} correspond to the vibration of P–O bond in $LiFePO_4$ [60,61]. Particularly, the characteristic Li–O absorption band bond at 498 cm^{-1} is weak, indicating the weak interaction between Li and O atoms, which enables Li^+ ions to insert/extract easily in the ordered olivine $LiFePO_4$ structure [54]. In Fig. 9c, weak bands situated at 1604 and 1656 cm^{-1} are also observed apart from those for the PO_4^{3-} absorption, which could be ascribed to the stretching vibration mode of the carbonyl of PVP. However, compared with the C=O adsorption position of pure PVP at 1679 cm^{-1} (Fig. 9b), this band evidently moves to a high wavenumber. Therefore this result confirmed not only the presence of PVP in the as-synthesized

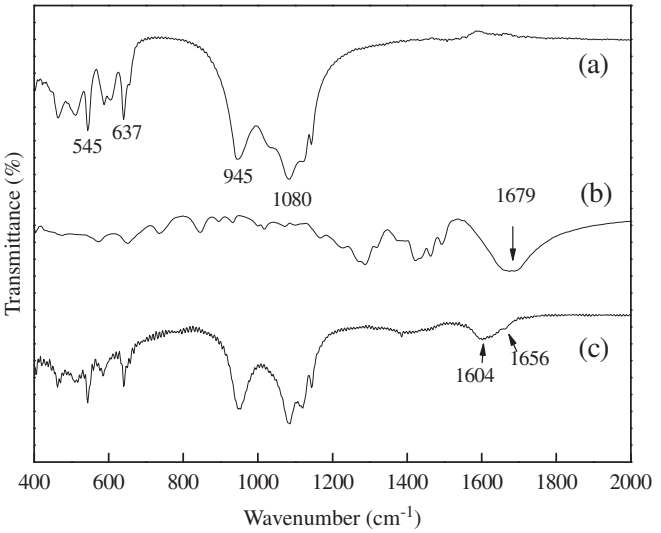

Fig. 9. FT-IR spectra of (a) pure $LiFePO_4$ sample without PVP, (b) pure PVP, and (c) $LiFePO_4$ microstructures obtained by the solvothermal process.

$LiFePO_4$, but also the interaction between the C═O (PVP) and the $LiFePO_4$ crystal surfaces, which is consistent with earlier studies [50,54].

Fig. 10a shows charge and discharge curves of the $LiFePO_4$/C microcomposite between 4.2 and 2.5 V at a current rate of 0.2 C for the first 10 cycles. The curves feature the typical electrochemical characteristics of the olivine-type $LiFePO_4$ cathode with a straightforward and flat charge and discharge plateau at around 3.46 and 3.40 V, respectively, which are identified as the two-phase redox reaction process via a first-order transition between $LiFePO_4$ and $FePO_4$ [3]. The coulombic efficiency (defined as the ratio of discharge capacity to charge capacity) of the initial cycle is a bit low, about 80%, but instantly increases to 99% in the subsequent cycles. After the 10th cycle, the coulombic efficiency retains 100%. Fig. 10b exhibits the cycling behavior of the $LiFePO_4$/C microcomposite at a 0.2 C rate. The initial discharge capacity is about 118 mAh g^{-1}, accompanied with a slightly increasing capacity fluctuation between 122 and 129 mAh g^{-1} on the first 10 cycles and then gradually leveling off at 124 mAh g^{-1} after 70 cycles. The irreversible capacity loss during the first cycle, good electrochemical reversibility after being activated by the initial reaction, and the reversible redox reaction being maintained up to 70 cycles without any obvious decay in the charge and discharge curves, indicate an utmost stable and reversible electrochemical reaction of the hierarchically fan-shaped $LiFePO_4$/C microcomposite.

The effect of carbon-coating (PVP) on the electrochemical properties of $LiFePO_4$ is shown in Fig. 11. It can be seen that the $LiFePO_4$/C microcomposite (with PVP) exhibits a capacity of about 118 mAh g^{-1} at the current rate of 0.2 C, which is clearly higher than 79 mAh g^{-1} for the pure $LiFePO_4$ without carbon (without PVP). With the carbon

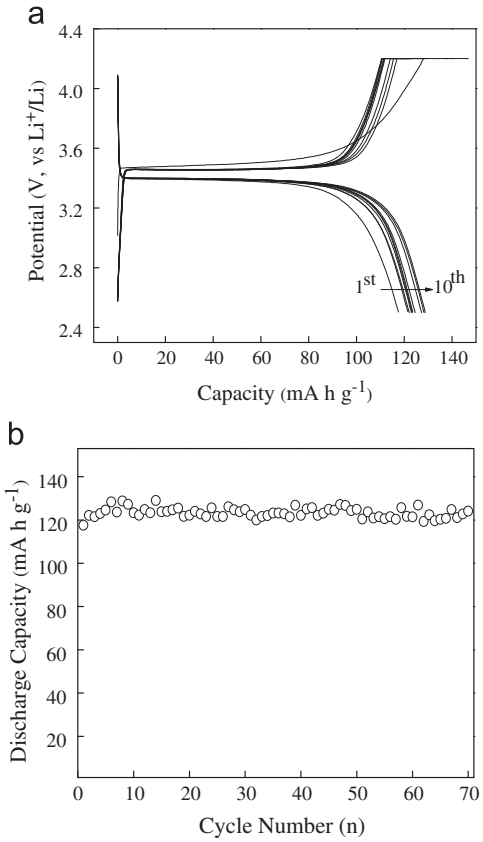

Fig. 10. (a) Charge and discharge profiles of the $LiFePO_4$ sample between 4.2 and 2.2 V at a current rate of 0.1 °C for the first 10 cycles, and (b) discharge capacity vs. cycle number of $LiFePO_4$ products after calcination at 0.1 C rate.

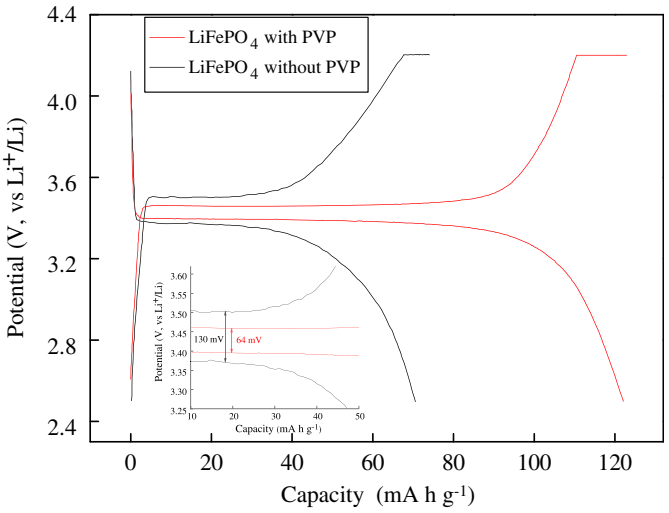

Fig. 11. The typical charge/discharge profiles of the synthesized $LiFePO_4$ with and without PVP at a charge/discharge rate of 0.1 C; the inset shows the flat region magnified.

coating, the polarization between the charge and discharge plateaus is reduced to 64 mV from 130 mV, which is for the sample without carbon, indicating that the kinetics of the $LiFePO_4$ is indeed improved due to the enhanced electronic conductivity resulted from the carbon coating. As is well known, an ideal LIB cathode material needs to be a mixed ionic and electronic conductor, but the olivine-phosphate is inherently a poor electronic and ionic conductor. This is one reason that the capacity of our synthesized $LiFePO_4$ microstructures is lower than corresponding theoretical capacity. Another possible reason may be that the size of our sample is relatively larger than those of reported literature [18,32,55,62], which is also a barrier for electrochemical reaction. However, the reduced diffusion length for lithium along one of the short dimensions (*b* axis) in the $LiFePO_4$ microplates enhances the ionic conductance. In addition, the nanoscale carbon layer networking of the microplates somewhat alleviates the problem of low electronic conductivity.

To provide more information for the improved electrochemical property, alternating current (AC) impedance measurements are conducted on $LiFePO_4$ with and without PVP electrodes at the same charge/discharge state (Fig. 12). The Nyquist plots consist of a semicircle and a straight line in the high- and low-frequency range. The high-frequency semicircle is ascribed to the interfacial charge-transfer impedance of electrochemical reaction and the straight line to the ion diffusion-controlled Warburg resistance [63,64]. By fitting the data of Fig. 12(a) with the equivalent circuit as displayed in Fig. 12b, it can be derived that the redox reaction resistance of $LiFePO_4$ without PVP is 100.5 Ω, and for the $LiFePO_4$ with PVP, the redox reaction resistance is 81.1 Ω. It indicates that the charge-transfer resistance of $LiFePO_4$ with PVP is lower than that of the $LiFePO_4$ without PVP. Therfore, based on the results in Fig. 12, we can conclude that the $LiFePO_4$ material with PVP becomes more conductive, which is also confirmed by the cell performance from Fig. 11. On the contrary, the electrochemical behavior for the solvothermal synthesized $LiMnPO_4$ and $LiCoPO_4$ (not shown) is completely different from that of $LiFePO_4$, although they are synthesized in the same way and have the same structural and morphological characteristics. The $LiMnPO_4$ sample has a specific capacity remaining over repeated cycles, but it is only a half of the capacity of $LiFePO_4$ at the same current rate of 0.1 °C. Such a result could be explained by the much lower intrinsic electronic conductivity of $LiMnPO_4$ and the strong cooperative Jahn–Teller lattice distortion at the Mn^{3+}, which causes an extreme instability of the crystalline phase $MnPO_4$

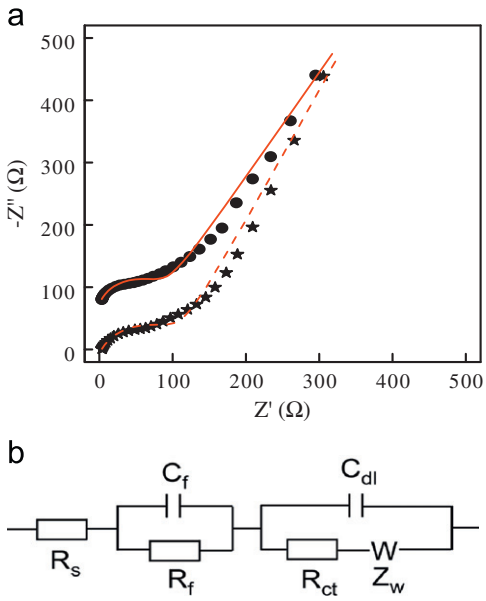

Fig. 12. (a) Nyquist plots of $LiFePO_4$ with and without PVP electrodes in the frequency range of 10 mHz to 100 kHz, ★ and ● represent $LiFePO_4$ without and with PVP, respectively. (b) Equivalent circuit model used for Nyquist plots fitting of $LiFePO_4$ with and without PVP electrodes.

produced after Li^+ extraction [65]. The $LiCoPO_4$ sample shows an extremely poor electrochemical performance with a rather low capacity, which is due to the lack of suitable electrolyte to operate at high voltage of 4.8 V.

Nevertheless, it must be addressed that our carbon-coated $LiFePO_4$ microstructures still exhibit significant performance in a lithium battery, although they possess undesirable larger grain size and thicker plates than the values in references [66–68], which most likely sacrifice the lithium ion diffusion coefficient and capacity delivery in some degree [69]. If the solvothermal conditions are optimized, carbon-coating $LiMPO_4$ samples with much smaller particle size have possibility to be obtained and better electrochemical properties would be achieved.

4. Conclusions

With a view of our findings, the general, facile, and one step solvothermal route offers a powerful method for direct synthesizing microstructured $LiMPO_4$ (M=Mn, Fe, and Co) series, using inexpensive and environmentally benign ethanol as the solvent, and PVP as the template and carbon source. This facile route features low-cost raw materials, mild reaction conditions, and simple manipulation to access well-crystalline and high-purity products generally with a length of several micrometers and a nanosized thickness, in which the short dimension is the diffusion direction. The electrochemical properties of $LiFePO_4$ microstructures with carbon coating are better than those of the sample without carbon, and this result is significant and acceptable for microstructured phosphates prepared in a fast one-step method at a moderate temperature. The excellent cycling performance makes it a promising electrode for lithium ion batteries.

Acknowledgments

This work was supported by the Natural Science Foundation of China (NSFC, nos. 20731002, 10876002, 20871016, 91022006, and 20973023), the 111 Project (B07012), Program for New Century Excellent Talents in University, Open Fund of State Key Laboratory of Explosion Science and Technology and Beijing Institute of Technology (nos. ZDKT08-01 and YBKT09-13), Specialized Research Fund for the Doctoral Program of Higher Education (SRFDP, nos. 200800070015 and 20101101110031), and Funding Project for Science and Technology Program of Beijing Municipal Commission (no. Z09010300820902). We thank the Fengyun Cui for structure drawing.

References

[1] H.F. Wang, Y.I. Jang, B.Y. Huang, D.R. Sadoway, Y.M. Chiang, J. Electrochem. Soc. 146 (1999) 473–480.
[2] J.F. Ni, H.H. Zhou, J.T. Chen, X.X. Zhang, Mater. Lett. 59 (2005) 2361–2365.
[3] A.K. Padhi, K.S. Nanjundaswamy, J.B. Goodenough, J. Electrochem. Soc. 144 (1997) 1188–1194.
[4] R. Amin, P. Balaya, J. Maier, Electrochem. Solid-State Lett. 10 (2007) A13–A16.
[5] D.Y.W. Yu, C. Fietzek, W. Weydanz, K. Donoue, T. Inoue, H. Kurokawa, S. Fujitani, J. Electrochem. Soc. 154 (2007) A253–A257.
[6] C. Delacourt, P. Poizot, M. Morcrette, J.M. Tarascon, C. Masquelier, Chem. Mater. 16 (2004) 93–99.
[7] K. Amine, H. Yasuda, M. Yamachi, Electrochem. Solid-State Lett. 3 (2000) 178–179.
[8] J. Yang, J.J. Xu, J. Electrochem. Soc. 153 (2006) A716–A723.
[9] F. Zhou, M. Cococcioni, K. Kang, G. Ceder, Electrochem. Commun. 6 (2004) 1144–1148.
[10] S.Y. Chung, J.T. Bloking, Y.M. Chiang, Nat. Mater. 1 (2002) 123–128.
[11] S. Shi, L. Liu, C. Ouyang, D.S. Wang, Z. Wang, L. Chen, X. Huang, Phys. Rev. B 68 (2003) 195108.
[12] H. Liu, Q. Cao, L.J. Fu, C. Li, Y.P. Wu, H.Q. Wu, Electrochem. Commun. 8 (2006) 1553–1557.
[13] S. Franger, F.L. Cras, C. Bourbon, H. Rouault, J. Power Sources 119–121 (2003) 252–257.
[14] J. Yang, J.J. Xu, Electrochem. Solid-State Lett. 7 (2004) A515–A518.
[15] M. Gaberscek, R. Dominko, J. Jamnik, Electrochem. Commun. 9 (2007) 2778–2783.
[16] N. Recham, M. Armand, L. Laffont, J.-M. Tarascon, Electrochem. Solid-State Lett. 12 (2009) A39–A44.
[17] Y. Wang, J. Wang, J. Yang, Y. Nuli, Adv. Func. Mater. 16 (2006) 2135–2140.
[18] X.L. Wu, L.Y. Jiang, F.F. Cao, Y.G. Guo, L.J. Wan, Adv. Mater. 21 (2009) 2710–2714.
[19] D. Rangappa, M. Ichihara, T. Kudo, I. Honma, J. Power Sources 194 (2009) 1036–1042.
[20] F. Croce, A. D'Epifanio, J. Hassoun, A. Deptula, T. Olczac, B. Scrosati, Electrochem. Solid-State Lett. 5 (2002) A47–A50.
[21] Y.S. Hu, Y.G. Guo, R. Dominko, M. Gaberscek, J. Jamnik, J. Maier, Adv. Mater. 19 (2007) 1963–1966.
[22] S.P. Herle, B. Ellis, N. Coombs, L.F. Nazar, Nat. Mater. 3 (2004) 147–152.
[23] G.T. Lei, X.H. Yi, L. Wang, Z.H. Li, J. Zhou, Polym. Adv. Technol. 20 (2009) 576–580.
[24] L.N. Wang, Z.C. Li, H.J. Xu, K.L. Zhang, J. Phys. Chem. C. 112 (2008) 308–312.
[25] D. Morgan, A. Van der Ven, G. Ceder, Electrochem. Solid State Lett. 7 (2004) A30–A32.
[26] M.S. Islam, D.J. Driscoll, C.A.J. Fisher, P.R. Slater, Chem. Mater. 17 (2005) 5085–5092.
[27] G.Y. Chen, X.Y. Song, T.J. Richardson, Electrochem. Solid State Lett. 9 (2006) A295–A298.
[28] A. Yamada, M. Hosoya, S.C. Chung, Y. Kudo, K. Hinokuma, K.Y. Liu, Y. Nishi, J. Power Sources 119–121 (2003) 232–238.
[29] H.M. Xie, R.S. Wang, J.R. Ying, L.Y. Zhang, A.F. Jalbout, H.Y. Yu, G.L. Yang, X.M. Pan, Z.M. Su, Adv. Mater. 18 (2006) 2609–2613.
[30] H.C. Kang, D.K. Jun, B. Jin, E.M. Jin, K.H. Park, H.B. Gu, K.W. Kim, J. Power Sources 179 (2008) 340–346.
[31] H. Gabrisch, J.D. Wilcox, M.M. Doeff, Electrochem. Solid-State Lett. 9 (2006) A360–A363.
[32] B. Ellis, W.H. Kan, W.R.M. Makahnouk, L.F. Nazar, J. Mater. Chem. 17 (2007) 3248–3254.
[33] K. Dokko, S. Koizumi, H. Nakano, K. Kanamura, J. Mater. Chem. 17 (2007) 4803–4810.
[34] W. Porcher, P. Moreau, B. Lestriez, S. Jouanneau, D. Guyomard, Electrochem. Solid-State Lett. 11 (2008) A4–A8.
[35] D. Rangappa, K. Sone, M. Ichihara, T. Kudo, I. Honma, Chem. Commun. 46 (2010) 7548–7550.
[36] D. Rangappa, K. Sone, T. Kudo, I. Honma, J. Power Sources 195 (2010) 6167–6171.
[37] A. Manthiram, A. Vadivel Murugan, A. Sarkar, T. Muraliganth, Energy Environ. Sci. 1 (2008) 621–638.
[38] A. Vadivel Murugan, T. Muraliganth, A. Manthiram, Electrochem. Commun. 10 (2008) 903–906.
[39] D. Wang, H. Buqa, M. Crouzet, G. Deghenghi, T. Drezen, I. Exnar, N.H. Kwon, J.H. Miners, L. Poletto, M. Grätzel, J. Power Sources 189 (2009) 624–628.

[40] A. Eftekhari, J. Electrochem. Soc. 151 (2004) A1456–A1460.
[41] I. Belharouak, C. Johnson, K. Amine, Electrochem. Commun. 7 (2005) 983–988.
[42] W.L. He, Y.C. Zhang, X.X. Zhang, H. Wang, H. Yan, J. Cryst. Growth 252 (2003) 285–288.
[43] Y. Ye, F.L. Yuan, S.H. Li, Mater. Lett. 60 (2006) 3175–3178.
[44] Z.G. Zhao, M. Miyauchi, J. Phys. Chem. C 113 (2009) 6539–6546.
[45] Z.S. Hu, L.Y. Li, X.D. Zhou, X. Fu, G.H. Gu, J. Colloid. Interf. Sci. 294 (2006) 328–333.
[46] Y.W. Wang, H.Y. Xu, H. Wang, Y.C. Zhang, Z.Q. Song, H. Yan, C.R. Wan, Solid State Ionics 167 (2004) 419–424.
[47] D. Fattakhova, V. Petrykin, J. Brus, T. Kostlanova, J. Dedecek, P. Krtil, Solid State Ionics 176 (2005) 1877–1885.
[48] K. Shiraishi, K. Dokko, K. Kanamura, J. Power Sources 146 (2005) 555–558.
[49] G. Ceder, F. Zhou, L. Wang, 212th the Electrochemical Society Meeting Abstracts, Washington, DC, 2007, Abs. nos. 636–640.
[50] S.I. Nishimura, G. Kobayashi, K. Ohoyama, R. Kanno, M. Yashima, A. Yamada, Nat. Mater. 7 (2008) 707–711.
[51] S. Suzuki, M. Tomita, S. Okada, H. Arai, J. Phys. Chem. Solids 58 (1997) 799–805.
[52] (a) A. Caballero, M. Cruz-Yusta, J. Morales, J. Santos-Pena, E. Rodeiguez-Castellon, Eur. J. Inorg. Chem. 9 (2006) 1758–1764;
(b) T. Baird, K.C. Campbell, P.J. Holliman, R.W. Hoyle, D. Stirling, B.P. Williams, M. Morris, J. Mater. Chem. 7 (1997) 319–330.
[53] (a) D.W. Choi, D.H. Wang, I.T. Bae, J. Xiao, Z.M. Nie, W. Wang, V.V. Viswanathan, Y.J. Lee, J.G. Zhang, G.L. Graff, Z.G. Yang, J. Liu, Nano Lett. 10 (2010) 2799–2805;
(b) Y.J. Zhao, S.J. Wang, C.S. Zhao, D.G. Xia, Rare Metals 28 (2009) 117–121.
[54] Y.G. Guo, J.S. Hu, L.J. Wan, Adv. Mater. 20 (2008) 2878–2887.
[55] A. Vadivel Murugan, T. Muraliganth, P.J. Ferreira, A. Manthiram, Inorg. Chem. 48 (2009) 946–952.
[56] W.Z. Ostwald, Phys. Chem. 34 (1900) 495–503.
[57] Y. Li, J. Liu, X. Huang, G. Li, Cryst. Growth Des. 7 (2007) 1350–1355.
[58] L. Suber, I. Sondi, E. Matijević, D.V. Goia, J. Colloid Interf. Sci. 288 (2005) 489–495.
[59] (a) S.F. Chen, S.H. Yu, T.X. Wang, J. Jiang, H. Colfen, B. Hu, B. Yu, Adv. Mater. 17 (2005) 1461–1465;
(b) Y.X. Gao, S.H. Yu, X.H. Guo, Langmuir 22 (2006) 6125–6129;
(c) N. Gehrke, H. Colfen, N. Pinna, M. Antonietti, N. Nassif, Cryst. Growth Des. 5 (2005) 1317–1319.
[60] C.M. Burba, R. Frech, J. Electrochem. Soc. 151 (2004) A1032–A1038.
[61] A.A. Salah, P. Jozwiak, K. Zaghib, J. Garbarczyk, F. Gendron, A. Mauger, C.M. Julien, Spectrochim. Acta Part A 65 (2006) 1007–1013.
[62] B. Kang, G. Ceder, Nature 458 (2009) 190–193.
[63] P. Suresh, A.K. Shukla, N. Munichandraiah, J. Appl. Electrochem. 32 (2002) 267–273.
[64] F. Nobili, F. Croce, B. Scrosati, R. Marassi, Chem. Mater. 13 (2001) 1642–1646.
[65] M. Yonemura, A. Yamada, Y. Takei, N. Sonoyama, R. Kanno, J. Electrochem. Soc. 151 (2004) A1352–A1356.
[66] K.F. Hsu, S.Y. Tsay, B.J. Hwang, J. Mater. Chem. 14 (2004) 2690–2695.
[67] N. Recham, L. Dupont, M. Courty, K. Djellab, D. Larcher, M. Armand, J.M. Tarascon, Chem. Mater. 21 (2009) 1096–1107.
[68] H. Yang, X.L. Wu, M.H. Cao, Y.G. Guo, J. Phys. Chem. C. 113 (2009) 3345–3351.
[69] A. Yamada, S.C. Chung, K. Hinokuma., J. Electrochem. Soc. 148 (2001) A224–A229.